Period Determination and Classification Analysis of Pulsating Red Giants

Anshita Saini, Nicholas Walker

s-sainia@bsd405.org; nwalker@bhusd.com

Abstract In this paper we present our updates and findings surrounding period and classification analysis of 21 Miras and 4 semiregular variables. Our primary methods for confirming pulsation period include both qualitative and quantitative examination of time series plots and light curves, along with cross-confirmation using publicly-accessible databases with over a hundred years of published data. Using the AAVSO's observations in both the Visual and Johnson V wavebands, and with the help of the AAVSO's VSTAR software, we arrived at refined period values to confirm data published by the VSX. Somewhat substantial updates are recommended for T UMi, though no other variables merited such sizable suggestions. Finally, the application of self-correlation studies provided further insight into the cycle-to-cycle changes in period and magnitude of semiregular variables.

1 Introduction

Pulsating red giants (PRGs) are radially-pulsating variable stars that occupy the ascending portion, along with the asymptotic giant branch (AGB), of the Hertzsprung-Russell Diagram. Stellar pulsation is typically caused by the expansion and contraction of the outer layers of such stars. Variables are classified into numerous categories according to factors like magnitude change and regularity of periodicity, the latter being the primary determinant of the *General Catalogue of Variable Stars* (GCVS; Samus et al. 2017) variability type. Mira variables, which have stellar features like those of the prototype Mira, o Ceti, have well-defined periods of around 100 to several hundred or up to 1,000 days. These periods may "wander" over time, a behavior studied in depth by Percy and Qiu (2019), Percy and Fenaux (2019), and Blackham (2020), though most Miras have regular, fundamental pulsation modes. Their magnitudes vary by 2.5 to 11 magnitudes in the visible waveband.

Semiregular variable stars display periodicity, but differ from Miras due to often ill-defined periods and characteristic irregularities. The periods of semiregular variable stars can range from 20 to over 2000 days, nearly twice those of longer-period Mira stars. Light amplitudes of semiregular stars vary as well, ranging from several hundredths to several magnitudes (GCVS). The SR stars presented in this paper exhibit a clear increasing or decreasing trend in light amplitude over time scales of several thousand Julian days. SRa stars similarly demonstrate periodicity and changing amplitudes and often exhibit light curves similar to Miras. However, SRa stars have smaller light amplitudes with more consistent magnitudes - generally under 2.5 V. Ranging from 25-1200 days, the periods of SRa stars are also more similar to the range of Mira periods than semiregular variable stars. SRb stars display poorly-defined periodicity and irregularities, somewhat distinguishing them from SR and SRa variable stars. The GCVS Catalogue assigns each SRb a mean period, though these stars often have two or more pulsating modes. The mean period range is similar to that of semiregular stars and ranges from 20 to 2300 days.

This project aims to confirm the periods and classifications of several semiregular variable stars and Mira variables through various methods of analysis on visual observations. Quantitative analysis of periodicity is presented through Fourier analysis and the Analysis of Variance algorithm. Confirming the classification of these stars was completed through qualitative analysis of light curves and self-correlation plots.

2 Resources

2.1 Variable Star Index (VSX)

The International Variable Star Index (VSX), developed for working groups of the American Association of Variable Star Observers (AAVSO) currently catalogues around 2 million variable stars (Watson et al. 2014). Each star in the catalog is updated with peer-reviewed information on its position, aliases, variability type, spectral type, magnitude range, and period, as well as links to relevant academic references. Many of the stars discussed in this paper may warrant updates in VSX, while others have been recently revised.

2.2 AAVSO International Database (AID)

The American Association of Variable Star Observers International Database (AAVSO's AID) contains nearly 50 million variable stars observations, including data points from over 100 years ago. The open-source database provided the visual and Johnson band observational data used to analyze both semiregular and Mira stars. As the largest and most comprehensive variable star database of its kind, it contains thousands of thoroughly reviewed observations contributed by various organizations and amateur astronomers around the world (Kafka 2019).

2.3 VSTAR

The AAVSO's VSTAR data visualization tool was used for period and magnitude analysis of the 25 chosen variable stars. The open-source application allows the user to generate light curves using data queried from AAVSO AID, as well as data from a variety of file types. VSTAR additionally offers the option of generating phase plots based upon a user-inputted period (Benn 2013). In addition to such diagrams, VSTAR offers multiple implementations of Discrete Fourier Transform analysis, including a "Standard Scan" or relying on a frequency or period range as provided by the user. Applying one of these three Fourier analysis options results in a "top hits" table, as well as a power spectrum (AAVSO 2018). Beyond Fourier analysis, VSTAR provides an implementation of the Analysis of Variance (AoV) algorithm, with an accompanying "top hits" table and periodogram.

3 Methods

3.1 DC DFT

We applied the Data-Compensated Discrete Fourier Trans-

form (DC DFT) algorithm in VSTAR to determine the periods of the variable stars presented in this paper. The DFT finds the Fourier coefficients assuming that a sinusoidal model fits the light curve. VSTAR's data-compensated algorithm ensures that gaps in the data are compensated for, yielding accurate analysis on both well sampled and poorly observed stars. In VSTAR, DC DFT determines the coefficient and associated "powers." The highest power levels indicate that the associated frequency is a likely candidate for the fundamental frequency of the data. These values are represented in the power spectrums below, with the x-axis as Frequency (Hertz) and the y-axis as the Power, or statistical significance, of each frequency.

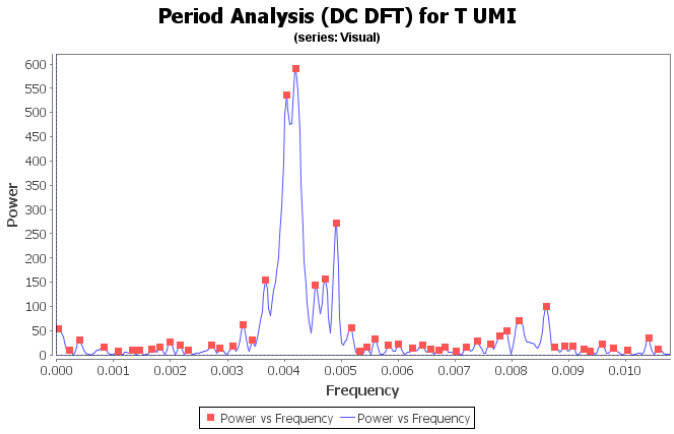

Figure 1. A power spectrum, or DC DFT plot, for SR variable T UMi from JD 2450000 to JD 2459200. Note the secondary peak at a frequency of approximately .004. This corresponds to what we believe to be a secondary pulsation mode.

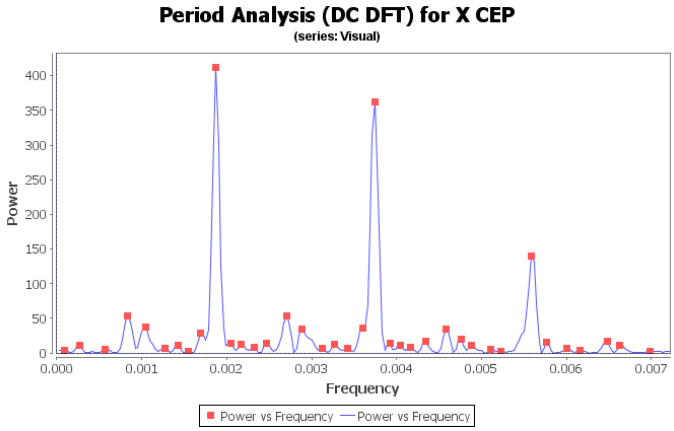

Figure 2. DC DFT plot for Mira X Cep. The power spectrum shows evident harmonic peaks at frequency intervals of approximately .002.

3.2 AoV

A second algorithm – Analysis of Variance (AoV) – was applied to confirm the period(s) found by DC DFT. Rather than Fourier analysis, this algorithm relies upon the One-way Analysis of Variance (ANOVA) algorithm to extract candidate periods. Upon inputting a period range based upon the DC DFT and VSX periods, VSTAR's AoV algorithm computes an F-statistic – indicating a statistical significance similar to the DC DFT power level for each candidate period, returning a periodogram of the F-statistic as a function of the period.

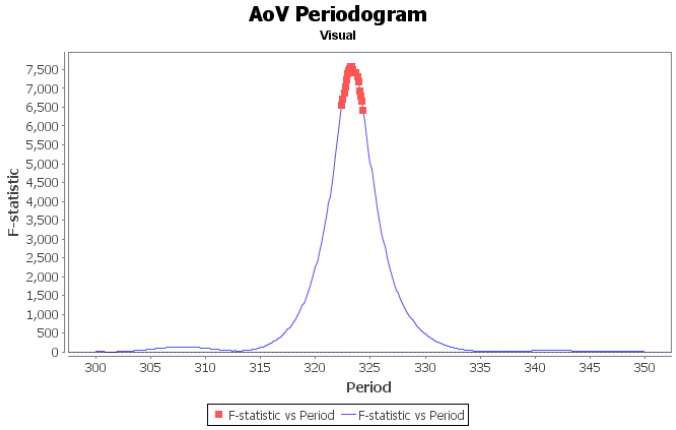

Figure 3. AoV Periodogram for Mira S UMi, from JD 2450000 to JD 2459200. The concentration of high F-statistic points indicates that the star is well-sampled, and that there is only a single strong candidate period.

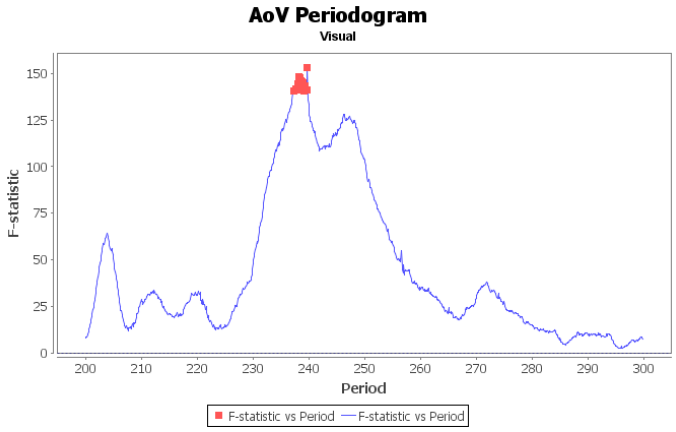

Figure 4. AoV Periodogram for T UMi, from JD 2450000 to JD 2459200. The peak of this plot at approximately 240 days coincides with the period in the self-correlation plot of T UMi (Figure 6).

3.3 Self-Correlation

To verify or suggest corrections and/or updates to the variability types of our subject stars (and as a tertiary form of period analysis), we applied the intuition of Percy and Kojar (2020), Percy and Mohammed (2004), and Percy and Ralli (1993) to develop our own self-correlation algorithm. The method is relatively straightforward: for all pairs of measurements in a given range of Julian Days (JD), which total to $\binom{N}{2}$ "coordinate points" of (JD, mag (V)), we calculate Δt and Δmagnitude (Δmag), appending these $\binom{N}{2}/2$ values to arrays of Δts and Δmags. After deciding on a "bin width" fit for each data set, typically around 10 JD, all Δts that fall within that range are averaged, along with the corresponding Δmag values. Absolute values are taken of any negative Δmag values beforehand, as we wish to focus on the absolute changes in cycle-to-cycle magnitude. We plot these averaged (Δt, Δmag) pairs in a "self-correlation diagram."

A change in period of the subject star, or sometimes a shift in amplitude, both of which — if in abundance — result in a non-constant-amplitude self-correlation diagram, and are sufficient to confirm or suggest semiregular variability. So, instead of visually inspecting our numerous light curves, we simply conduct a

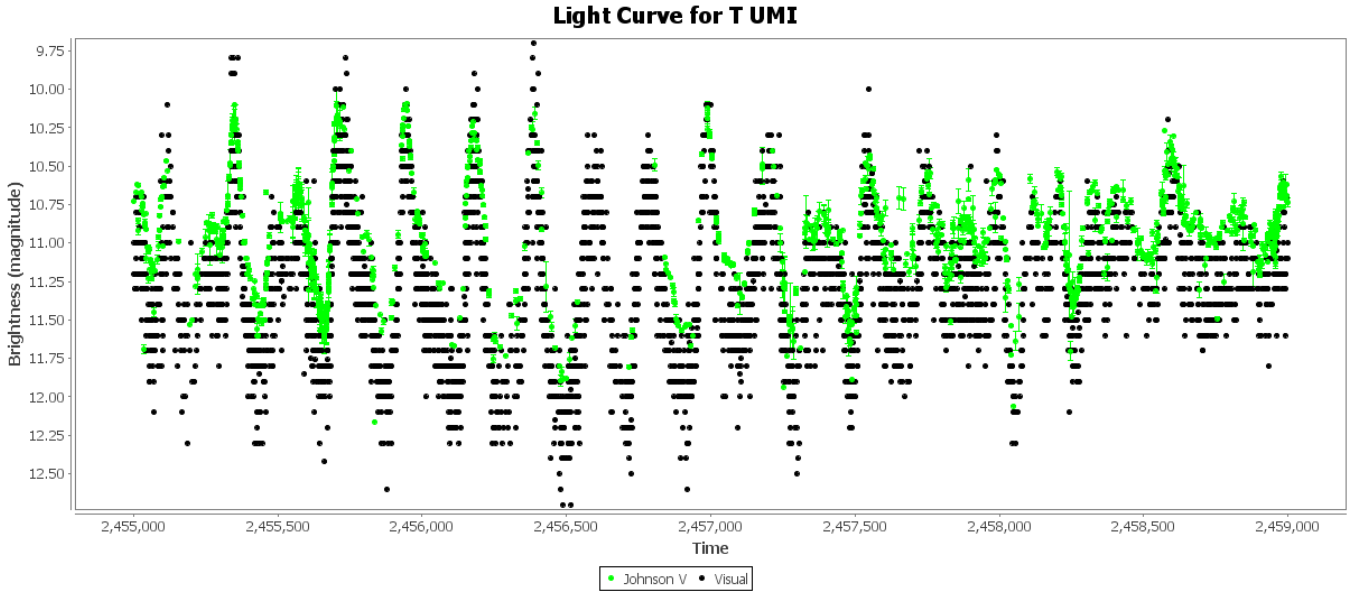

Figure 5. Light curve of T UMi generated from VSTAR. The decreasing magnitude serves as an ancillary confirmation of the star's classification as a semiregular.

visual analysis of a self-correlation plot, as shown in Figures 6-9. A range of average Δt = 0JD to average Δt of 1000JD serves as a good benchmark for detecting trends in self-correlation amplitudes. However, the behavior of the plot changes noticeably when selecting different time periods of the same JD range, maintaining a bin width of 10JD. Such differences are discussed in reference to our specific plots.

The relative minima of self-correlation diagrams, in most cases, reflect primary pulsation periods for Mira stars, and often for SR variables as well, although such minima tend to be changing in average self-correlation magnitude. We quantitatively confirmed the periods of the majority of our subject stars, with the exception of some poorly-sampled stars with harmonics in their time series.

In some of our self-correlation diagrams, the final few peaks seem to exhibit irregular behavior. This trend is not due to intrinsic properties of the subject star, but is rather an artifact of running the algorithm; simply, the frequency of Δt values decreases as Δt increases, and as such, delta mags are more sparse on the plot. The self-correlation diagram of RY Dra illustrates this phenomenon to some.

4 Results

Although the majority of our analyses just provided confirmations of the VSX values in Table 1, we did encounter numerous subject stars that exhibited deviations from the VSX data—particularly differences in period. Further, we also make not of several trends or irregularities that we observed while conducting our analyses.

The stars with asterisked DC DFT periods exhibit one or more harmonic periods that are almost exactly $\frac{1}{N}$ times the fundamental period. RW And, TX Cam, and Y Cep have respective harmonic periods of 215.554743, 166.861686, and 279.8797941 days. X Cep has a harmonic of 267.0 and a third harmonic of 178.9 days. These harmonics are not caused by actual pulsations of a variable star, but are rather higher-frequency artifacts (Percy and Golaszewska 2020).

X UMi, although it has more than two thousand observations in both the Visual and Johnson V bands, has poorly dispersed data, as observations are clustered together, resulting in a light curve that lacks periodicity and consistency. However, after running both DC DFT and AoV analyses for different JD ranges, we arrived at period values consistent enough to suggest an update to X UMi's period in VSX, from 388 days to 339 days.

Finally, T UMi, which we soon discuss in more depth, exhibited a period of approximately 237.5 days and a secondary pulsation mode with period 247.6 days, a substantial change from the period of 115.7 days listed in VSX. Our period was confirmed by both the Fourier routine and the variance analysis.

4.1 T UMi

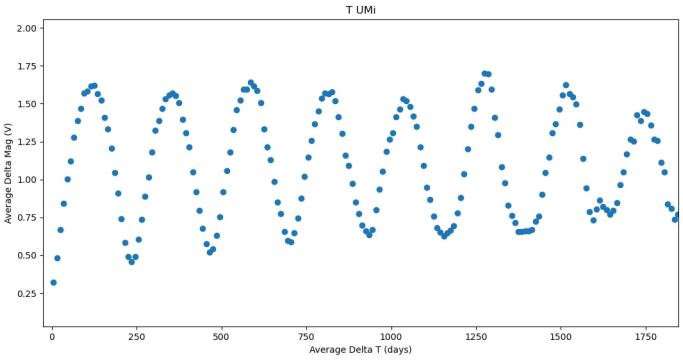

Figure 6. Self-correlation plot for T UMi (JD 2452000 - JD 2454000). The amplitude of average magnitude clearly decreases.

Here we demonstrate the "optimal" self-correlation diagram of a well-observed SR variable — that is, almost perfectly periodic and having a steadily changing amplitude — T UMi. The amplitude of the curve — that is, the distance from maxima to minima of average delta mag — is evidently decreasing, hinting at typical semiregular behavior. It is important to note, however, that a decreasing self-correlation amplitude is not the sole indication of semiregularity. As we will discuss with regard to other SR type stars, abnormal correlation diagrams — whether defined

Name	GCVS Type	VSX Period (days)	VSX Mag Range (V)	DC DFT Period (days)	AoV Period (days)	Mag Range (V)
R And	M	409.2	5.8 - 15.2	407.4	409.4	5.7 - 15.4
RW And	M	430.0	7.9 - 15.7	431.1*	431.5	7.7 - 17.4
V And	M	256.4	9.0 - 15.2	237.3	258.2	18.4 - 15.4
R Cam	M	270.22	6.97 - 14.4	270.1	269.6	7.8 - 14.2
T Cam	M	369.3	7.2 - 14.4	375.9	275.8	7.3 - 14.4
TX Cam	M	558.7	7.8 - 16.9	559.8*	555.7	7.7 - 15.8
AU Cam	SRa	366.0	10.0 - 10.7	363.5	363.7	9.0 - 11.4
R Cas	M	430.5	4.7 - 13.5	435.3	433.2	3.7 - 14.2
S Cas	M	608.2	7.9 - 17.3	613.6	611.3	8.0 - 17.5
T Cas	M	440.0	6.9 - 13.0	444.1	442.5	7.3 - 12.3
W Cas	M	407.9	8.2 - 13.0	406.4	405.1	8.1 - 13.3
S Cep	M	484.4	6.6 - 12.5	482.3	482.0	6.1 - 11.5
T Cep	M	388.1	5.2 - 11.3	385.9	384.6	5.0 - 11.5
Y Cep	M	332.6	8.1 - 16.0	332.0*	333.6	8.0 - 15.5
X Cep	M	535.2	8.1 - 17.5	533.9	533.7	8.0 - 15.6
R Dra	M	245.6	6.7 - 13.2	247.5	247.5	5.9 - 14.0
RY Dra	SRa	300.0:	5.88 - 8.0	276.8	276.7	5.7 - 8.4
T Dra	M	422.2	7.2 - 13.5	420.5	422.5	8.4 - 14.0
U Dra	M	316.1	9.1 - 14.6	318.7	319.0	8.8 - 14.6
W Dra	M	278.6	8.9 - 15.4	286.6	287.0	9.0 - 15.8
R UMi	SR	325.7	8.5 - 11.5	324.3	324.4	8.2 - 11.5
S UMi	M	331.0	7.5 - <13.2	323.9	323.3	7.4 - 13.0
T UMi	SR	115.7	7.8 - 15.0	237.5, 247.6	239.7	9.1 - 14.2
U UMi	M	330.9	7.1 - 13.0	324.1	323.9	7.4 - 12.5
X UMi	M	388.0	12.5 - 18.4**	339.2	338.8	11.5 - 16.1

Table 1: * denotes the presence of a harmonic period. The ** designates a magnitude range under photographic passband. The : is a symbol used by the VSX to indicate an uncertain value.

by a lack of periodicity or a wildly-changing amplitude — may also provide a fair basis for concluding semiregularity.

4.2 R UMi

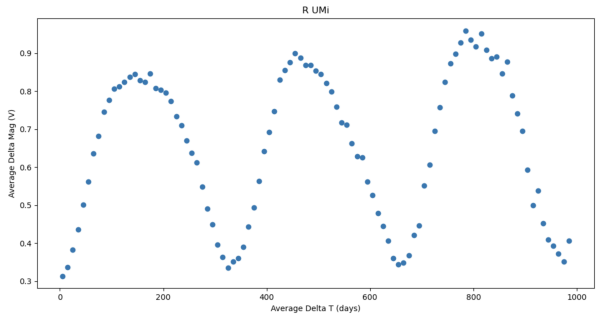

Figure 7. Self-correlation plot for R UMi (2451000 - 2452000 Julian Days) with consistent periodicity and an increasing amplitude.

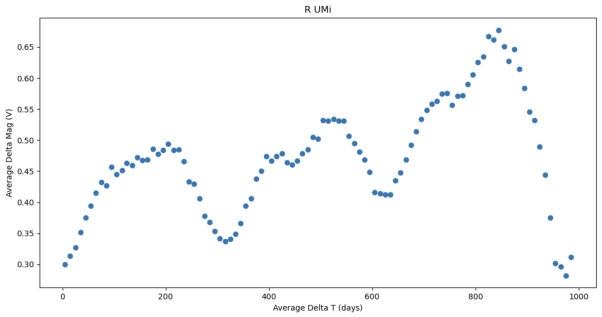

Figure 8. Shifted self-correlation plot for R UMi (JD 2452000 - 2453000). The difference in the periodicity of this plot as compared to the previous JD range indicates a possible secondary pulsation mode.

The above plots of R UMi reflect the changing behavior of this star across varying Julian Day time ranges. Such irregular periodicity is characteristic of a semi-regular variable star, confirming the VSX variability type of an SR. In addition, the magnitude range decreases from 0.3 – 0.9 V to 0.3 – 0.65 V. Plots of additional Julian Day time shifts have been omitted for brevity, but generally confirm a decreasing average magnitude for R UMi. Though the upper plot reflects a clear primary period, the peaks in the lower plot suggest the potential presence of two pulsation modes. However, both the primary and secondary periods are larger than the typical periods of a Cep(B) or RR(B) star, further confirming that the variability type of SR is the most likely classification.

4.3 RY Dra

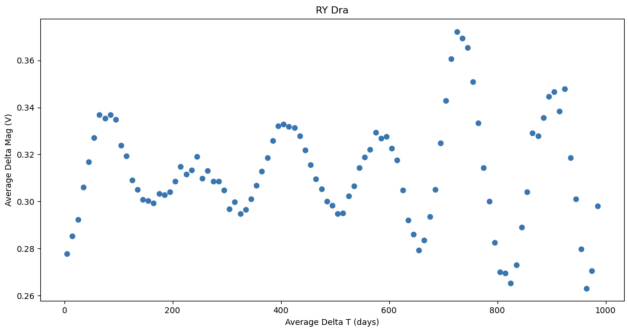

Figure 9. Self-correlation plot for RY Dra (2453000 - 2454000 Julian Days). This plot exhibits clear irregularity when compared to the previous self-correlation plots of SR and SRa stars.

As a semi-regular giant, RY Dra displays irregular periodicity and magnitudes, even over cycles of 6 periods, as well as the presence of two or more pulsation modes in self-correlation plots. This behavior coincides with its classification as an SRb star, which are generally characterized by poorly defined periodicity and irregular changes. As in the case of R Umi, the plots of various different Julian Day time shifts display a changing magnitude. RY Dra has both increasing and decreasing magnitude ranges with an increasing time range.

4.4 AU Cam

The period of AU Cam is 363.6 days, at or near a period of one year. Upon a cursory glance, it appeared that this year long period may have been a result of the seasonal Ceraski effect, briefly described by Percy et al. (2009). This effect causes a different perception of the magnitude difference between two stars due to the changing orientation of the star field throughout the year. The self-correlation diagrams of AU Cam depict that the period of one year is likely spurious. Moreover, the DC DFT power spectrum depicts a peak at a frequency of 0.000011 Hz with an amplitude nearly 6 times that of the 363.6 day period, similar to the behavior of the stars analyzed by Percy (2015). In accordance with Percy's conclusions, aliasing of the AU Cam's VLF variability is likely a cause of the one-year period.

5 Conclusion

Our study served to substantiate the existing characterizations and key stellar attributes, namely pulsation amplitude, GCVS variability type, and period, which we confirm via a number of analytical methods. The one standout case is T UMi, which appears to exhibit two pulsation modes of similar periods, though it is important to note that our proposed periods are not necessarily the most likely; the JD range that we selected for our DC DFT and AoV analysis of T UMi was one that produced results with minimal noise in the time series curve. Nevertheless, we are sure that T UMi's period has increased appreciably since its last update in the VSX.

Our self-correlation analysis provided no surprising updates to the variability types of SR variables T UMi, RY Dra, and AU Cam, though we emphasize the versatile nature of analyses of this sort. We also show how period and amplitude change through pulsation cycles, and how selecting different time scales reveals peculiar trends, specifically in the self-correlation plots of SR variables.

6 Acknowledgements

We thank the observers and the AAVSO staff team for the data used in this research, as well as the developers of the VSTAR software package. We additionally relied upon the International Variable Star Index (VSX) database. We are also grateful to Dr. John R. Percy and Dr. Adam W. Rengstorf for providing insight regarding period analysis with self-correlation.

References

AAVSO. 2018, *Variable Star Classification and Light Curves Manual*, version 2.4, AAVSO, Cambridge, Mass.

Benn, D. 2013, VSTAR data analysis software (http://www.aavso.org/vstar-overview).

Blackham, J. 2020, *J. Amer. Assoc. Var. Star Obs.*, 48, 111.

Kafka, S. 2020, Observations from the AAVSO International Database (https://www.aavso.org).

Percy, J. R. 2015, *J. Amer. Assoc. Var. Star Obs.*, 43, 176.

Percy, J. R. et al. 2009, *J. Amer. Assoc. Var. Star Obs.*, 37, 71.

Percy, J. R., and Fenaux, L. 2019, *J. Amer. Assoc. Var. Star Obs.*, 47, 202.

Percy, J. R., Golaszewska, P. 2020, *J. Amer. Assoc. Var. Star Obs.*, 48, 165.

Percy, J. R., Kojar, T. 2013, *J. Amer. Assoc. Var. Star Obs.*, 41, 15.

Percy, J. R., and Mohammed, J. 2004, *J. Amer. Assoc. Var. Star Obs.*, 32, 9.

Percy, J. R., and Qiu, J. 2019, *J. Amer. Assoc. Var. Star Obs.*, 47, 76.

Percy, J. R., and Ralli, J. 1993, *Publications of the Astronomical Society of the Pacific*, 105, 287.

Samus, N. N., Kazarovets, E. V., Durlevich, O. V., Kireeva, N. N., and Pastukhova, E. N., 2017, Astron. Rep., 61, 80, General Catalogue of Variable Stars: Version GCVS 5.1 (http://www.sai.msu.su/gcvs/gcvs/index.htm).

Watson, C., Henden, A. A., and Price, C. A. 2014, AAVSO International Variable Star Index VSX (Watson, 2006– 2014; http://www.aavso.org/vsx).